DRDC Ottawa SL 2004-032

Reprinted from:
Proceedings EUSAR 2004. May 25-27
p. 819-822

APPLYING FRACTIONAL FOURIER TRANSFORM TO TWO-APERTURE SAR-GMTI

Shen Chiu and Ishuwa Sikaneta

Space-Based Radar Group, Radar Systems Section,
Defence R&D Canada - Ottawa
3701 Carling Ave., Ottawa, ON, Canada, K1A 0Z4

ABSTRACT

SAR along-track interferometry (SAR-ATI) can be used to measure motion in a scene by utilizing the phase and magnitude information of the interferogram. The phase of a target's interferogram $\Delta\phi$ is, to first order, proportional to its slant range velocity v_r at broadside. Due to the nature of SAR data collection, the moving target signal is unavoidably contaminated by the scene clutter. Depending on the signal-to-clutter ratio (SCR), the velocity and the azimuth shift estimated from the phase may have significant errors. The proposed technique applies the so-called fractional Fourier transform (FrFT) to improve the SCR in order to reduce the clutter contamination effect on the interferometric phase. By mapping a target's signal onto a fractional Fourier axis, its energy can be highly compressed, at same time filtering out most of the interfering clutter. Two-channel airborne SAR data were used for this study. Results show that the proposed method is an effective and elegant way of accurately estimating velocity and position parameters.

1 INTRODUCTION

Canada's RADARSAT-2 commercial SAR satellite, to be launched in Fall 2005, will have an experimental mode (called MODEX for Moving Object Detection EXperiment) that will allow two portions of the full antenna aperture to be used with two parallel receivers to define two independent data channels [1]. These two sub-apertures, arranged to lie along the flight path, enable one to detect targets with non-zero radial velocity by providing essentially two identical views of the observed scene but at slightly different times. It can be shown that a moving target with a slant range velocity v_r causes a differential phase shift $\Delta\phi = 4\pi v_r \tau/\lambda$ (τ is the time between two observations), which may be detected by interferometric combination of the signals from a two-channel along-track SAR system [2]. The interferometric phase $\Delta\phi$ is often used to estimate a target's radial velocity and azimuth shift, without considering the fact that its phase is corrupted by the overlapping stationary clutter (cf. [3]). This may lead to serious errors in velocity and position estimates. This paper applies the so-called Fractional Fourier Transform (FrFT) to filter out the interfering background clutter as much as possible in order to provide a "cleaner" target signal for the interferometric phase estimation. With the classical Fourier transform, the signal is projected onto the frequency axis. The FrFT, on the other hand, projects the signal onto a rotated frequency axis (or fractional frequency space), allowing a moving target's chirp signal to be highly concentrated in this fractional Fourier domain and, hence, to be easily extracted. Airborne along-track SAR data are used for this study. Results show that the FrFT is a more effective and elegant technique for clutter filtering than the time-frequency approach previously proposed by the first author [4]. The method is shown to significantly improve the target velocity and position estimation.

2 FRACTIONAL FOURIER TRANSFORM

The fractional Fourier transform (FrFT) with rotational angle α of a signal $f(t)$ is defined as [5] [6]

$$F_\alpha(u) = R^\alpha[f](u) = \int_{-\infty}^{\infty} f(t) K_\alpha(t,u)\,dt, \qquad (1)$$

where for α not equal to zero or a multiple of π, the kernel $K_\alpha(t,u)$ is given by

$$K_\alpha(t,u) = \frac{c}{\sqrt{2\pi}} e^{ja[(t^2+u^2)-2but]}, \qquad (2)$$

and

$$a = \frac{\cot\alpha}{2}, \quad b = \sec\alpha, \quad c = \sqrt{1 - j\cot\alpha}. \qquad (3)$$

The FrFT with parameter α can be considered as a generalization of the conventional FT. Thus, the FrFT for $\alpha = \pi/2$ and $\alpha = -\pi/2$ reduces to the conventional and inverse FT, respectively. Multiplying both sides of (1) by e^{-jau^2}, one obtains

$$\begin{aligned} e^{-jau^2} F_\alpha(u) &= \widetilde{F}_\alpha(u) \\ &= \frac{c}{\sqrt{2\pi}} \int_{-\infty}^{\infty} f(t) e^{ja(t^2-2but)}\,dt. \end{aligned} \qquad (4)$$

Substituting $u/(2ab)$ for u in (4), it becomes

$$\begin{aligned} \widetilde{F}_\alpha\left(\frac{u}{2ab}\right) &= \frac{c}{\sqrt{2\pi}} \int_{-\infty}^{\infty} f(t) e^{j(at^2-ut)}\,dt \\ &= \frac{1}{\sqrt{2\pi}} \int_{-\infty}^{\infty} \{c f(t) e^{jat^2}\} e^{-jut}\,dt \\ &= \frac{1}{\sqrt{2\pi}} \int_{-\infty}^{\infty} g_\alpha(t) e^{-jut}\,dt = G_\alpha(u). \end{aligned} \qquad (5)$$

The last line in (5) shows that the FrFT is a variation of the standard Fourier transform. As such, many of its properties, such as its inverse formula and sampling theorems for band-limited and time-limited signals, can be easily derived from those of the Fourier transform by a simple change of

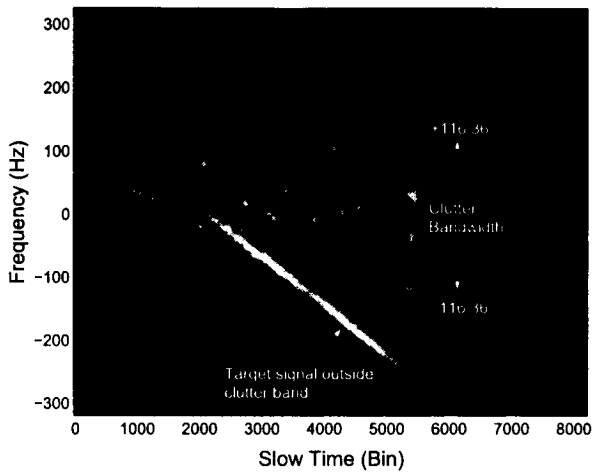

Figure 1: *Time-frequency plot, using short-time Fourier transform, of target 8 (T8) showing the Doppler-shifted linear chirp of the target overlaid on stationary back ground clutter (3 dB beamwidth also shown).*

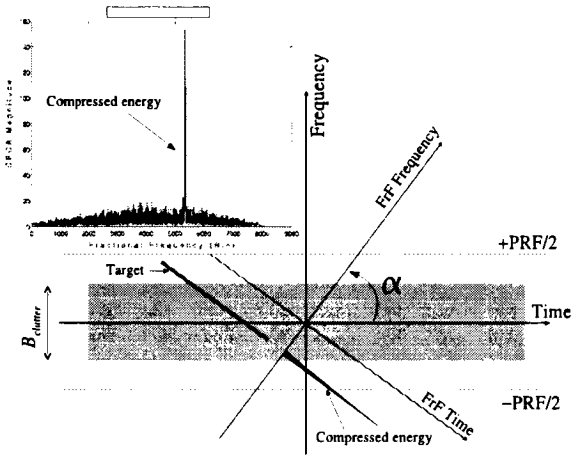

Figure 2: *Illustrating a target energy focused via the FrFT. The insert shows an actual moving target's (T10) signal compressed in the fractional frequency domain.*

variable. With respect to the parameter α, the FrFT is continuous, periodic ($R^{\alpha} = R^{\alpha+2\pi n}$, with n an integer) and additive ($R^{\alpha}R^{\beta} = R^{\alpha+\beta}$), and has the symmetry relation $R^{\alpha}[f^*](u) = \{R^{-\alpha}[f](u)\}^*$. The inverse FrFT can thus be written as

$$f(t) = R^{-\alpha}[F_{\alpha}](t) = \int_{-\infty}^{\infty} F_{\alpha}(u)K_{-\alpha}(t,u)du. \quad (6)$$

Figure 1 shows the time-frequency (TF) plot, obtained via the short-time Fourier transform (STFT) technique [7], of a measured moving target signal (T8; see Figure 3) superimposed on a stationary background clutter. The target's range-compressed signal is a linear chirp in "slow time" (or azimuth), which appears as a slanted line in the TF plane. Because of the target's across-track velocity component v_y, the signal is shifted in frequency (in this case in the negative direction). If the target has an along-track velocity component v_x, its energy will be rotated slightly in the TF-plane with respect to a stationary point target. The signal remains a linear chirp as long as the target has no along-track acceleration component a_x or other higher order terms.

Gierull [3] has shown theoretically that the peak of the marginal phase density function of a moving target's interferogram migrates from zero (stationary clutter) towards its true Doppler phase (introduced by its radial velocity) for an increasing SCR. The FrFT maps the signal onto a rotated (or fractional) frequency axis such that the originally slanted chirp energy becomes perfectly perpendicular to the rotated axis and, thus, highly localized as illustrated in Figure 2. Also shown in Figure 2 (insert) is a measured moving target (T10) mapped onto the optimum fractional frequency axis. The target energy, as can be seen, is highly compressed. Note that the clutter has been suppressed via the Displaced Phase Center Antenna (DPCA) technique [8]. The residual clutter (plus noise) surrounding the signal chirp can be further filtered out (if so desired) and, at the same time, the signal strength is dramatically increased. The result is a significant improvement in the SCR and, thus, in the phase estimation accuracy. This mapping process is equivalent to the SAR azimuth compression via a matched filter that matches to the target along-track velocity v_x. The signal compression via the FrFT is not sensitive to across-track velocity v_y, in contrast to the matched filter approach, and would lead to a fully focused target if it is moving at a constant velocity throughout the synthetic aperture time or only accelerating in the across-track direction. Unlike a matched filter that completely models the target's motion, the FrFT cannot, in principle, fully focus a target accelerating in along-track direction (i.e. $a_x \neq 0$) because a_x introduces nonlinearity in the signal chirp. The across-track acceleration, on the other hand, only introduces a linear Doppler shift in the chirp and, therefore, does not cause nonlinearity [9].

3 AIRBORNE EXPERIMENT

As part of the preparatory work for the RADARSAT-2 MODEX, airborne experiments were conducted to acquire SAR-ATI data for typical RADARSAT-2 resolutions and incident angles. The data set used in this study was obtained at Canadian Forces Base (CFB) Petawawa on November 5, 2000, by the Environment Canada CV 580 C-band SAR configured in its along-track interferometer mode. The study focuses on targets of opportunity (TOOs) on Highway 17, which runs through the experimental site. The highway was monitored by two video cameras 600 m apart set up along a stretch of the highway to measure TOO speeds. The highway has a speed limit of 90 km/h, but most TOOs monitored were 10-20 km/h over the speed limit. The video cameras monitored over 47 vehicles during the data acquisition period, and their monitored ground speeds v_g varied from 83 km/h to 120 km/h.

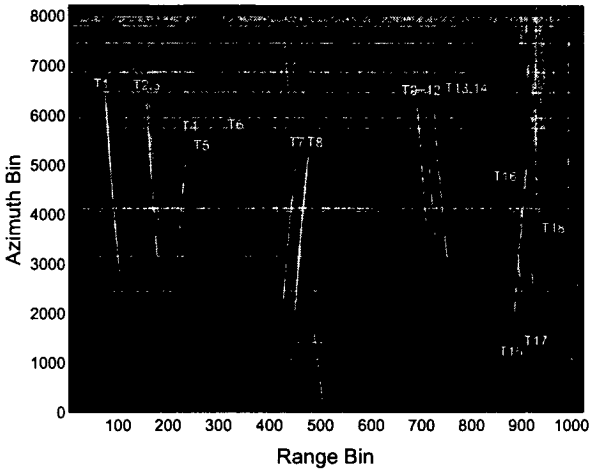

Figure 3: *Range-compressed raw-data DPCA output. The horizontal lines are due to motion compensation artifacts.*

4 RAW-DATA TARGET DETECTION

Targets were detected in the range-compressed raw data domain via a combination of the DPCA technique [8], which subtracts the aft-aperture image from the (co-registered) fore-aperture image to suppress the background clutter, and the raw-data target detection algorithm developed by Gierull and Sikaneta [10] [11]. The DPCA is first applied to the pair of fore and aft channel range-compressed signal data to obtain an "image" of target track history as shown in Figure 3. Since the targets are azimuthally uncompressed, their energies spread over the slow time. Since these targets are moving on Highway 17, their track histories are slanted in range as seen in Figure 3, indicating range walk. Uncancelled bright stationary targets also show up in the image, as seen in the upper right-hand corner of Figure 3 (where a small town is located), but their tracks are always vertical. In order to estimate the target parameters, Gierull and Sikaneta's [10] automatic detection algorithm is first used to extract their signal tracks. Eighteen targets were detected and analyzed.

5 VELOCITY/POSITION ESTIMATION

Having detected the targets and extracted their tracks, each target is individually analyzed via the following parameter estimation algorithm. The FrFT is first applied to each target to maximize its SCR by mapping its energy onto a fractional Doppler domain. This is done by scanning through the angular parameter α as in (1) to maximize the SCR. Then the ATI phase is computed for this optimum fractional angle α to get the "best" (or the least contaminated) ATI phase $\Delta\phi$. The radial velocity v_r at the broadside (also equal to the slant range velocity) is computed from the interferometric phase $\Delta\phi$ using the relationship [12]

$$v_r = \frac{\Delta\phi\lambda}{4\pi\tau}, \tag{7}$$

where τ is the time delay between the pair of received signals. The ground range velocity v_y is calculated from $v_y = v_r/\sin\eta$, where η is the incident angle. The along-track velocity v_x, on the other hand, is estimated from the fractional (or rotational) angle α, which can be obtained from (1) by setting it equal to a delta function $\delta(u)$ (i.e. the target energy is fully focussed):

$$F_\alpha(u) = \int_{-\infty}^{\infty} e^{-j\frac{4\pi R(t)}{\lambda}} K_\alpha(t,u)dt = \int_{-\infty}^{\infty} e^{j2\pi ut}dt = \delta(u), \tag{8}$$

where $R(t)$ is the moving target's range history. Solving (8) for α, one obtains the relationship:

$$\alpha = \cot^{-1}\left\{\frac{2N}{R_b\lambda f_s^2}\left[(v_x - v_a)^2 + v_y^2(1 - y_0^2/R_b^2)\right]\right\} \tag{9}$$

or

$$v_x = v_a - \sqrt{\frac{R_b\lambda f_s^2\cot\alpha}{2N} - v_y^2\left(1 - \frac{y_0^2}{R_b^2}\right)}, \tag{10}$$

where R_b and y_0 are the slant range and the ground range of the target at broadside, respectively, v_a is the platform velocity, N is sample length, and f_s is the sampling (or pulse repetition) frequency. The target azimuth shift correction can be computed from

$$\Delta x = \frac{v_y v_a y_0}{(v_x - v_a)^2 + v_y^2} \approx \frac{v_y y_0}{v_a} = \frac{v_r R_b}{v_a}, \tag{11}$$

where the approximation is valid only when $v_a \gg v_x, v_y$. Equations (9)-(11) assume a non-accelerating target in a flat-earth geometry.

Figure 4 shows the polar plots of three (T4, T9, and T10) of the eighteen detected targets' interferograms. Figures 4(a)-4(c) are interferograms obtained from the regular SAR-ATI processing (i.e. from the fore and aft SAR images processed by the stationary terrain matched filter). Interferograms for the same targets obtained from the FrFT processing are shown in Figures 4(d)-4(e). The signal points near the zero phase radial belong to the stationary clutter. As can be seen, ATI phases obtained from the regular SAR processing are severely contaminated by the interfering clutter and their values are completely off. The FrFT, on the other hand, not only gives much cleaner and well defined phases but also correct values compared to their true phases. The "true" phase is here defined to be the $\Delta\phi$ that gives the correct azimuth shift to bring a target back onto the road (or Highway 17). The analysis results of all eighteen targets are summarized in Table 1, which shows targets' interferometric phases $\Delta\phi$ and their estimated ground velocities v_g. The velocities and azimuth shifts of 10 targets are correctly estimated by the FrFT approach compared to only three by the regular SAR approach.

Figure 5 plots the targets' azimuthally corrected positions estimated from the proposed FrFT approach. The circles represent targets in their azimuth-shifted positions and the squares are their corrected locations. As can be seen, ten out of eighteen targets are correctly positioned on Highway 17. The other targets are off because their SCRs remain small ($\lesssim -3$ dB) even after the FrFT processing.

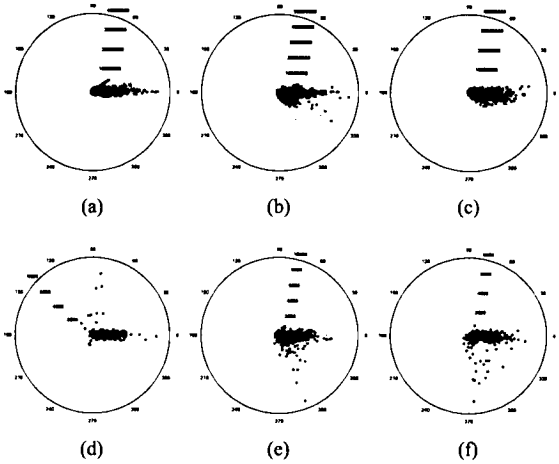

Figure 4: *(a) - (c) are clutter-corrupted ATI signals for targets T4, T9, and T10 respectively; (d) - (f) are the same targets' ATI signals after the FrFT filtering or focussing.*

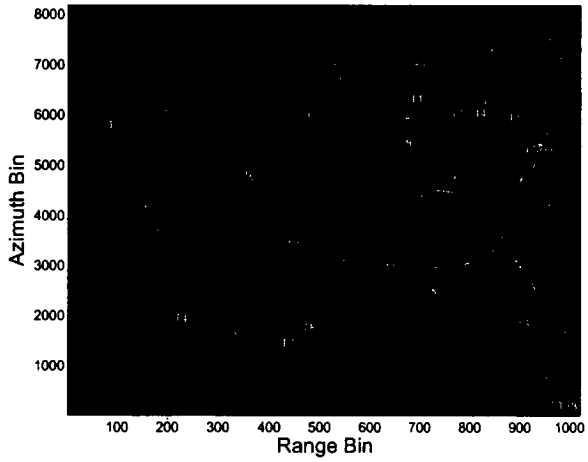

Figure 5: *Detected moving targets in the SAR image context. The circles represent target azimuth-shifted positions and the squares are azimuth-corrected positions.*

Table 1: *Estimated interferometric phase $\Delta\phi$ and ground velocity v_g of eighteen detected targets.*

Target ID	SAR $\Delta\phi$[°] / v_g[km/h]	FrFT $\Delta\phi$[°] / v_g[km/h]	"True" $\Delta\phi$[°] / v_g[km/h]
T1	−142/104.5	−132.7/106.2	−131/106.5
T2	−42/118.9	−42.8/118.7	−43/118.7
T3	0/0	−87/110.7	−157.7/98.4
T4	+32/118.7	+80/110.4	+79/110.6
T6	−60/110.4	−71/108.5	−71.3/108.5
T7	+106/100.8	+103/101.3	+100/101.8
T8	+88/103.2	+85.4/103.6	+85/103.7
T9	−26/110.7	−65/104.5	−63.5/104.7
T10	−30/109.9	−85/101.1	−84/101.3
T11	−5/113.8	−70/103.4	−104.5/98.0
T12	0/0	−135/93.0	−137/92.7
T13	−60/104.2	−10/112.1	−83/100.6
T14	−47/106.0	−48/105.9	−86.5/99.8
T15	+30/124.7	+45/122.0	+44/122.2
T16	−32/124.4	−130/106.7	−150/103.1
T17	0/0	−82/115.0	−153.5/102.2
T18	0/0	+44/120.8	+98.5/111.0

6 SUMMARY

A two-channel SAR along-track interferometer (SAR-ATI) was used to measure motion in a scene. The target radial velocity at the broadside was estimated from the interferometric phase $\Delta\phi$. Due to the nature of SAR measurements, the target signal is contaminated by the scene clutter. The FrFT technique was applied to increase the SCR and to improve the accuracy of target parameter estimation. By mapping a target's signal onto a fractional Fourier domain, its energy can be highly focussed, at same time filtering out most of the interfering clutter. Results showed that the proposed method is an effective and elegant way of reducing clutter contamination and of accurately estimating velocity and position parameters.

7 REFERENCES

[1] Livingstone, C.E. 1998. The Addition of MTI Modes to Commercial SAR Satellites. In Proc. of 10th CASI Conference on Astronautics, Ottawa, Canada, 26-28 October 1998.

[2] Raney, R.K. 1971. Synthetic aperture imaging radar and moving targets. IEEE Transactions on Aerospace and Electronic Systems, AES-7(3), pp. 499-505.

[3] Gierull, C.H. 2002. Moving target detection with along-track SAR interferometry. Technical Report TR 2002-084, Defence R&D Canada - Ottawa, August.

[4] Chiu, S. 2003. Clutter effects on ground moving target velocity estimation with SAR along-track interferometry. In IGARSS'2003, Proceedings of the International Geoscience and Remote Sensing Symposium, Toulouse, France, 21-25 July.

[5] Almeida, L.B. 1994. The fractional Fourier transform and time-frequency representations. IEEE Trans. Signal Processing, Vol. 42, No.11, pp. 3084-3091.

[6] Zayed, A.I. 1996. On the relationship between the Fourier and fractional Fourier transforms. IEEE Trans. Signal Processing Letters, Vol. 3, No. 12, pp. 310-311.

[7] Boashash, B. 2003. Heuristic formulation of time-frequency distributions. In *Time Frequency Signal Analysis and Processing*, Elsevier, pp. 38-41.

[8] Dickey, F.R., Jr., Santa, M.M. 1953. Final report on anticlutter techniques, General Electric Company Rept. R65EMH37, 1 Mar. 1953.

[9] Sharma, J.J. and Collins, M.J. 2004. Focusing accelerating ground moving targets in SAR imagery. In this conference (EUSAR 2004).

[10] Gierull, C.H. and Sikaneta, I.C. 2003. Raw Data based Two-Aperture SAR Ground Moving Target Indication. In IGARSS'2003, Proceedings of the International Geoscience and Remote Sensing Symposium, Toulouse, France, 21-25 July 2003.

[11] Gierull, C.H. and Sikaneta, I.C. 2004. Ground moving target parameter estimation for two-channel SAR. In this conference EUSAR 2004.

[12] Raney, R.K. 1992. Special SAR techniques and applications. In AGARD Lecture Series 182 on Fundamentals and Special Problems of SAR, AGARD-LS-182, pp. 10-1 to 10-15.

#S22074

CA0244496